PAPER • OPEN ACCESS

Freely suspended smectic films with in-plane temperature gradients

New Journal of Physics
The open access journal at the forefront of physics

Deutsche Physikalische Gesellschaft DPG
IOP Institute of Physics

Published in partnership with: Deutsche Physikalische Gesellschaft and the Institute of Physics

OPEN ACCESS

RECEIVED
5 April 2019

REVISED
10 May 2019

ACCEPTED FOR PUBLICATION
3 June 2019

PUBLISHED
21 June 2019

PAPER

Freely suspended smectic films with in-plane temperature gradients

Ralf Stannarius[1], Torsten Trittel[1], Christoph Klopp[1], Alexey Eremin[1], Kirsten Harth[1,2], Noel A Clark[3], Cheol S Park[3] and Joseph E Maclennan[3]

[1] Institute of Experimental Physics, Otto von Guericke University, D-39106 Magdeburg, Germany
[2] Universiteit Twente, Physics of Fluids and Max Planck Center for Complex Fluid Dynamics, PO Box 217, 7500 AE Enschede, The Netherlands
[3] Soft Materials Research Center, Physics Department, University of Colorado, Boulder, CO 80309, United States of America

E-mail: ralf.stannarius@ovgu.de

Keywords: Marangoni flow, freely suspended thin fluid films, smectic liquid crystals, microgravity

Supplementary material for this article is available online

Abstract

Freely suspended smectic films with in-plane temperature inhomogeneities can exhibit remarkable thermocapillary (Marangoni) effects. The temperature dependence of the surface tension $\sigma(T)$ promotes flow in the film plane, convection roll patterns, and climbing of smectic layers against gravitational forces. We discuss several experimental geometries where macroscopic material transport is driven by temperature gradients, including experiments under normal gravity and observations in microgravitation during suborbital rocket flights and on the International Space Station. In all these experiments, the temperature dependence of the surface tension drives unidirectional material flow. The divergence of this flow near the hot and cold film edges, and at the boundaries of film islands in the film, is associated with the creation, motion and removal of dislocations. These dissipative processes limit the flow velocity.

1. Introduction

Liquid crystals (LCs) play a dominant role in display technology today, and their unique ferroelectric, pyroelectric and flexoelectric properties make them attractive for many other applications such as sensors and actuators. Yet their importance goes far beyond technical interest: they are uniquely suited to studying the fundamental physics of complex fluids. Freely suspended films with aspect ratios reaching 10^6:1 formed by some smectic phases can be considered as quasi two-dimensional (2D) fluids, where flow is restricted to the film plane. Their huge surface to volume ratio (reaching an order of up to 10^8 m^{-1}) makes these structures very susceptible to capillary forces, and in particular to forces related to the temperature dependence of surface or interface tensions. Here, we will describe several experiments in which thermally driven flow is observed in such quasi-2D liquids.

Since the first descriptions of smectic freely suspended films about 40 years ago [1, 2], they have been a rich source of scientific discoveries. Manifold studies have been devoted to understanding the structure, fluctuations and phase transitions in these films [3–6], hydrodynamic phenomena, and director field structures [7–12] as well as spontaneous pattern formation [13–15]. The dynamics and spontaneous self-organization of inclusions such as islands (regions of excess smectic layers) and droplets have been investigated [16–20]. Other interesting aspects are shape transformations [21–24] and rupture processes [24–27]. All of these types of experiments have been performed under nominally homogeneous temperature conditions.

A few studies have focused on the effects of thermal gradients on smectic freely suspended films. Godfrey and van Winkle exposed horizontal films in vacuum to temperature gradients in the film plane [28], and were able to detect convection rolls in gradients as low as 0.032 K mm^{-1}. Their experimental geometry is sketched in figure 1(a). The films had a length (along the heated/cooled edges) of 9.3 mm and width (gap between the thermocontacts) of 3.1 mm. The film menisci played a decisive role in the convective flow of these films. A surprising aspect of their interpretation of the experimental observations is that they needed to assume a positive

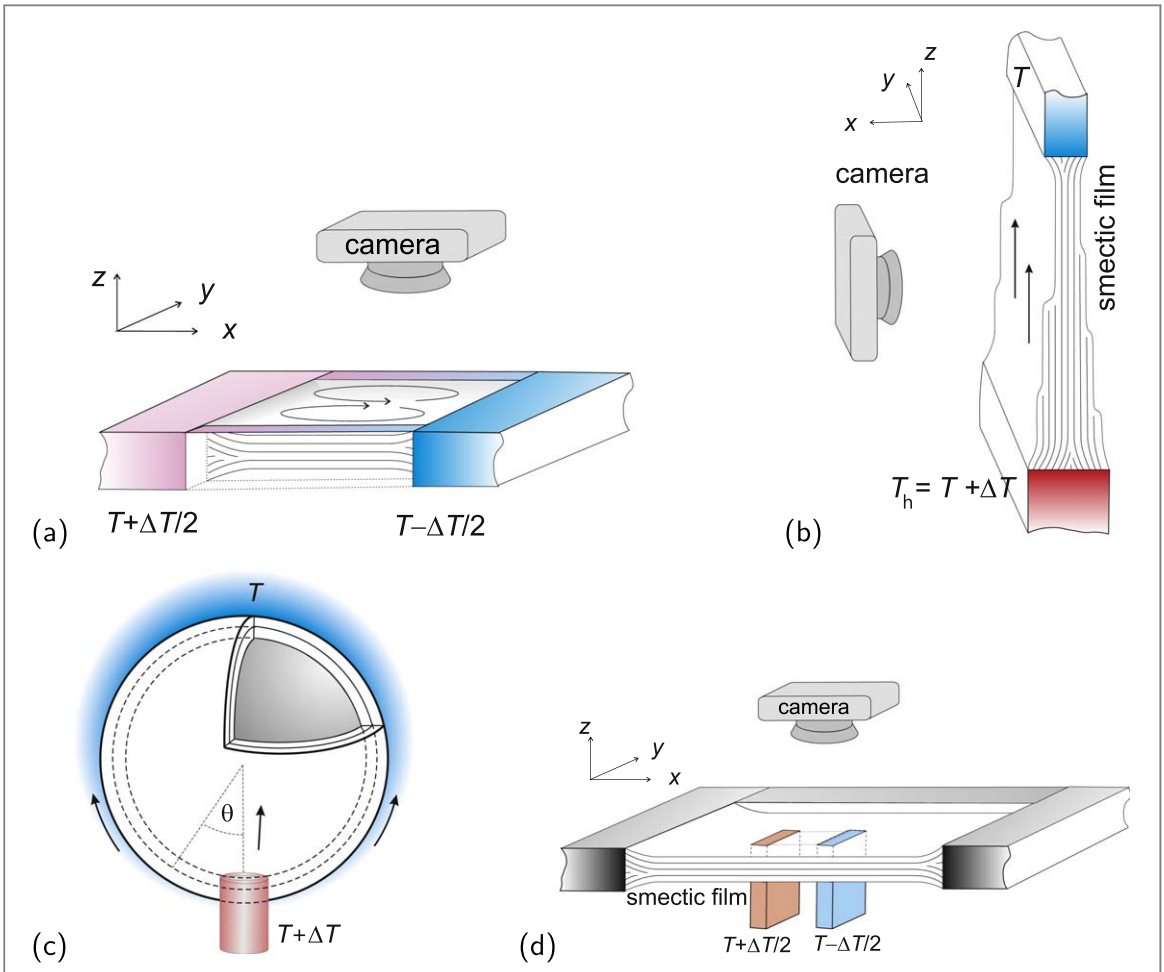

Figure 1. The four experimental geometries discussed in this paper. (a) Experiment of Godfrey and van Winkle in vacuum at normal gravity [28]. The convection rolls are indicated by arrows. The horizontal film was in contact with two opposite edges of the frame that could be heated to defined temperatures. The sides of the frame connecting the two thermocontacts were covered by menisci. (b) Vertical frame used in Birnstock's experiments [30]. (c) Bubble with heated support needle on the ISS (the needle tip is not to scale). (d) Frame with thermocontacts used in the TEXUS 52 and TEXUS 55 suborbital rocket missions [32]. The front edge of the frame is omitted for better clarity. Layer thicknesses are greatly exaggerated.

temperature gradient of the surface tension. Such an anomaly has indeed been found in some smectic phases. However, the material they used (Schiff's base DOBAMBC) definitely has a negative temperature coefficient $\mathrm{d}\sigma/\mathrm{d}T < 0$ throughout the smectic A and C phases [29]. Thus, their interpretation of the convection mechanism appears to be ill-founded.

Birnstock and Stannarius investigated vertical smectic films heated from below [30]. In addition to the climbing of smectic layers upwards against gravity, they observed convection rolls in the thinnest (submicrometer thick) regions of the film. Both phenomena are discussed in detail in section 2.3 below. The convection rolls were caused by a buoyancy-driven, thermoconvective instability (of Rayleigh–Bénard type) of the ambient air. The thin smectic film acts only as a sensitive indicator of surrounding air flow. The geometry of Birnstock's experiment is shown in figure 1(b). Film widths and heights were in the range of several centimeters. Layer climbing was not the focus of that study, and its physical origin was not addressed by the authors.

Transport processes in thin smectic films driven by thermal gradients have also been investigated in microgravity (μg) experiments on the International Space Station ISS [31]. Smectic bubbles about 15 mm in diameter and with film thicknesses of a few nanometers were created on a thin support needle 1.27 mm in diameter. This needle was then heated to a temperature above the ambient air temperature in the surrounding chamber (figure 1(c)). In these experiments, smectic islands (see sketch in figure 2) in the film were found to migrate away from the heated needle, towards the opposite pole of the bubble.

A decisive step forward in the quantitative understanding of thermocapillary flows in thin smectic free-standing films was achieved by Trittel *et al* [32] in the analysis of microgravity experiments during suborbital rocket flights. This experimental geometry is shown in figure 1(d). The rectangular 'thermopads' inserted into the film far from the support frame and from the film meniscus provided a temperature gradient in the smectic film plane. The pads had cross sections of $5 \times 1\ \mathrm{mm}^2$, and were separated by 2.5 mm. The total film area was

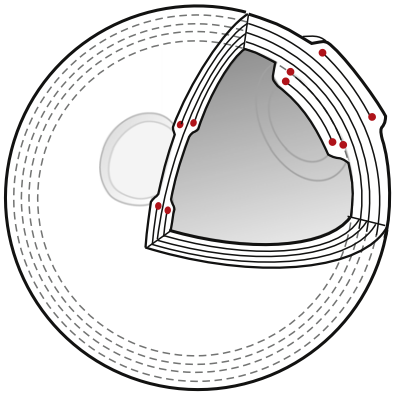

Figure 2. Sketch of smectic islands and holes in a bubble-shaped film. The layer thicknesses are greatly exaggerated. Layer dislocations surrounding islands and holes are marked by red dots.

$13 \times 10\ \mathrm{mm}^2$. Heating the film with the metal pads at different temperatures created macroscopic flow against the temperature gradient, from the hot pad to the cold one, as expected for materials with negative temperature coefficient of the surface tension. A model developed to explain this motion as Marangoni flow predicts that the motion sets in with practically no threshold in this experiment.

The purpose of the present paper is an analysis and comparison of the above-mentioned experiments. First we analyze the experiment with planar films in weightlessness, performed during the TEXUS 52 suborbital flight. Then we describe qualitatively the effects of thermal gradients in the geometry of spherical smectic bubbles supported by a heated needle in microgravity, including the transport of inclusions in the films. Finally, we discuss inhomogeneously thick, vertical films in normal gravity, and explain qualitatively the observed layer climbing phenomenon.

2. Experimental observations

2.1. Drift and convection rolls in flat films under zero gravity

In the TEXUS 55 experiment, with the geometry sketched in figure 1(d), freely suspended smectic films were exposed to temperature gradients of up to $10\ \mathrm{K\ mm}^{-1}$. The liquid-crystalline material was 5-n-Decyl-2-(4-n-octyloxyphenyl) pyrimidine (*SYNTHON Chemicals*), here referred to as 10PP8. Its mesomorphism is Isotropic 69 °C Nematic 65 °C SmA 60 °C SmC 33 °C Cryst. A detailed analysis of the heat currents and flow fields in this experiment led to the following conclusions.

(1) The flow of the film from the hot to the cold thermocontact shifts the temperature profile in the film towards the cold contact (in material with $\mathrm{d}\sigma/\mathrm{d}T < 0$), so that the film heats up a few mK relative to a non-flowing film. This global temperature elevation is proportional to the flow velocity.

(2) The reduction of surface energy resulting from this temperature change is much larger than the kinetic energy necessary to move the film and adjacent air layers with the observed velocities.

(3) The flow velocity is roughly proportional to the temperature difference between the hot and cold edges, and flow sets in practically without threshold.

(4) Reversal of the gradient reverses the flow direction immediately.

(5) The shear gradients in the air adjacent to the film contribute only marginally to the energy dissipation: the processes that limit the acceleration of the flow occur in the menisci. Stress generated in the menisci opposes inflow and outflow of smectic film material. The stress is related to the flow velocity by a material constant, the mobility m of layer dislocations.

(6) The efficiency of this process is inversely proportional to the film thickness.

In the earlier TEXUS 52 experiment, the same experimental setup was used. A film of 535 nm thickness was exposed to temperature gradients between zero and $10\ \mathrm{K\ mm}^{-1}$. Figure 3 shows the temperature protocol and snapshots of the film between the thermocontacts. A gradient of $6\ \mathrm{K\ mm}^{-1}$ was already present during the film preparation (by drawing a metal edge from left to right across the support frame). Figure 3(a) shows the film

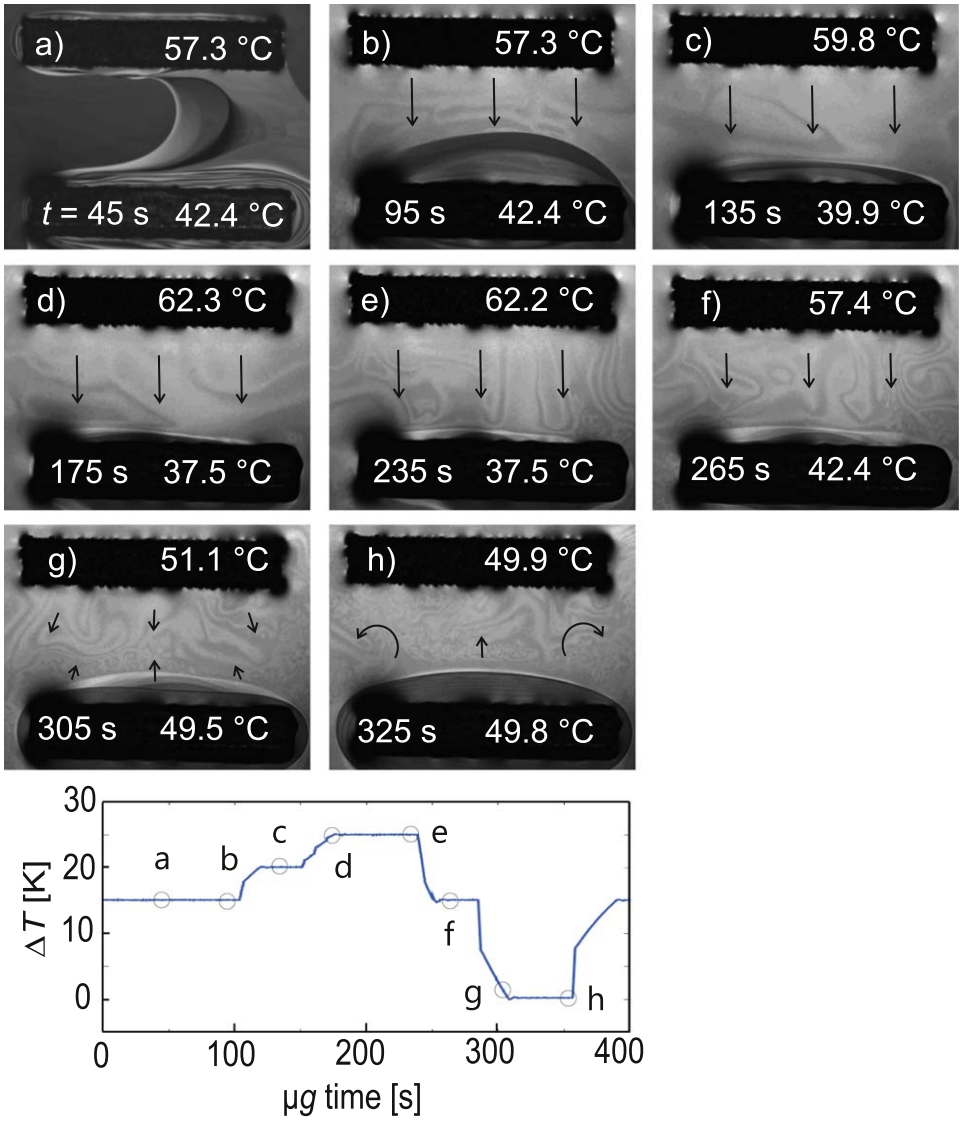

Figure 3. Textures observed during the TEXUS 52 flight: (a) smectic material (10PP8) collects at the cold pad already during film preparation, caused by thermocapillary flow along the drawing edge, (b) a wedge-shaped region of excess smectic material has formed around the cold pad. The remaining film is uniformly thick, material flow against the temperature gradient is driven by Marangoni forces, (c), (d) flow pushes the wedge towards the cooler pad, increasing the wedge angle, (e) material at the hot pad reaches the SmA phase, and the maximum achievable gradient is reached, (f), (g) the flow against the thermal gradient decreases with decreasing temperature gradient, competing with an expansion of the wedge zone. Two vortices appear at the sides of the region between the pads, (h) circulatory flows create shear and lead to a grainy texture of the c-director. The interference fringes in the wedge zone indicate that the region is at least 2 μm thick near the pad. Arrows sketch the local flow direction, image sizes are 6.0 $\times$ 4.8 mm^2. The graph at the bottom shows the temperature protocol in the microgravity phase.

immediately after preparation. It is initially inhomogeneous but not yet equilibrated: the film is about 1 μm thick at the right hand side and it has its final thickness in the region moving in at the left.

A consequence of the temperature gradient during preparation was a drift of material towards the colder pad. The collected material formed a wedge-shaped bulge of up to 2 μm thickness around that pad. During the following phase, until 4:00 min, thermocapillary flow transported more film material from the hot to the cold edge. This is reflected in the drift of the Schlieren texture (see video in the supplementary material, available online at stacks.iop.org/NJP/21/063033/mmedia). At the maximum temperature gradient of 10 K mm^{-1} ($\Delta T = 25$ K), the film near the hot pad was already SmA, where the Schlieren texture vanishes. The flow of material into the wedge compressed this region, and it became steeper and narrower, as seen in figures 3(b)–(e). The border of the bulge moved somewhat more slowly than the film, at about 15 μm s^{-1} in a gradient of 6 K mm^{-1} and at about 20 μm s^{-1} after the gradient was increased to 8 K mm^{-1}. In this process, the dislocations in the wedge were pushed closer together (reaching an estimated dislocation density of about 3 per μm).

After the temperature gradient was reduced again to 6 K mm^{-1}, the wedge relaxed and expanded again. As a consequence of the counterflow, the film texture acquired a grainy appearance. In addition, the film developed a convection roll pair at the edges of the field of view (figure 3). We note, however, that the physical mechanism of

this convection cannot be related to Rayleigh–Bénard or Bénard–Marangoni convection. The former is not effective because of zero gravity, the latter would require the backflow of cold material to the hot pad in order to form vortices. Here, the smectic material is stacked near the cold edge.

The limited microgravity time prevented the further observation of the convection structure. In consequence of the evaluation of the experimental data, we modified the design of the experiment in the follow-up mission TEXUS 55. There, the film was drawn under isothermal conditions, and neither of the two pads showed an agglomeration of material after film preparation. The results of this experiment were reported in [32].

The observations made during the TEXUS flights can be explained as follows. In a film of uniform thickness h, the relation between the observed drift velocity v and the temperature difference ΔT between the two contacts is

$$v = \frac{m\Sigma\Delta T}{h}, \tag{1}$$

with the dislocation mobility m, a material constant of the order of 4×10^{-8} m Pa^{-1} s^{-1} [33], and the temperature coefficient of the surface tension $\Sigma = \mathrm{d}\sigma(T)/\mathrm{d}T$. When Σ is negative as in most fluids (exceptions are mentioned in [32]), this flow is directed against the temperature gradient, from the higher temperature to the lower temperature regions.

Dislocations in the smectic layer structure, as seen in figure 1(b), occur wherever there are inhomogeneities of the film thickness. When the film material flows into the meniscus, new dislocations are created and pushed into the meniscus. The specific energy dissipation rate per unit length of the meniscus is $\phi_m = hv^2/m$, where h is the film thickness and v is the velocity of the material flowing into the meniscus [7].

Note that the flow velocity in equation (1) is independent of the distance between the two thermocontacts, unlike Rayleigh–Bénard convection where the Rayleigh number as the control parameter depends upon the gap width between the hot and cold plates cubed, or Bénard–Marangoni convection where the control parameter depends linearly upon the gap width (see, e.g. [34]).

When the film is laterally confined by a frame and meniscus, stress is generated by the flow of smectic material into and out of the menisci. When the film is inhomogeneously thick, as in the region near the cold pad in the TEXUS 52 experiment, the flow creates stress at the border of the bulging region at the cold plate, which pushes this border towards the cold edge. The corresponding force per length, $2\Sigma\Delta T$ is of the order of 1.5×10^{-3} N m^{-1} in our experiment. This leads to the compression of the wedge in figures 3(b)–(e). In a fixed temperature gradient, the equilibrium shape of the wedge, i.e. its stationary thickness gradient and the dislocation density, is established by the balance of the above-mentioned force and the repulsive forces between the dislocations in the wedge region. When the temperature gradient in the film is lowered, the stress decreases and thus the wedge angle relaxes, pushing the border back, away from the solid pad, as seen in figures 3(f)–(h). The dislocation density in the wedge has dropped to about $1/\mu$m in figure 3(h), and the wedge angle has relaxed to approximately 0.15°. The temperature difference was reset to 15 K again at time 6:00 min, shortly before the end of the microgravity phase, but a novel retraction of the wedge border could not be recorded since the film was destroyed shortly afterwards by acceleration forces during re-entry of the rocket.

2.2. Thermomigration of islands on smectic bubbles

Microgravity experiments with smectic bubbles were performed on the ISS in the framework of the OASIS project between August 2015 and March 2016. While most of the OASIS experiments were conducted in a uniformly thermostated chamber, a few experiments were devoted to exploring the effects of thermal gradients. For this purpose, the supporting needle could be set to a higher temperature than that of the chamber. It is difficult to estimate the resulting temperature profile in the chamber, so that we can provide only a qualitative discussion of the observed phenomena shown in figure 4. The material used was a smectic A mixture (8CB + Displaytech MX 12160 [31]), with phase sequence Isotropic 56 °C Nematic 54 °C SmA 5 °C Cryst. The uniformly thin bubble with a film thickness of a few smectic layers (10–20 nm) was first decorated with small islands (approximately 80 nm thick), which were created using airjets [31]. Then the needle temperature was set to 40 °C, with a nominal background temperature of the chamber walls of 28 °C. After a few seconds, as the temperature gradient in the surrounding air built up, the islands started to migrate away from the needle.

In microgravity, there is no buoyancy-driven thermal convection of the air in the chamber. The smectic bubble itself is an excellent indicator of convective flow of the air. The absence of noticeable flow patterns in the films suggests that the air can be considered as stationary. Thus, there is no significant heat transport by air flow. We can safely assume that the contribution of the thin smectic membrane itself to heat transport is also negligible. The temperature profile is thus established predominantly by heat diffusion in the air. The temperature distribution in the chamber may be estimated by solving the Laplace equation with appropriate boundary conditions at the needle and the chamber walls. We assumed an axially symmetric geometry (1.25 mm diameter needle held at 40 °C inside a cylindrical chamber with 25 mm radius). The solid line in figure 5 shows

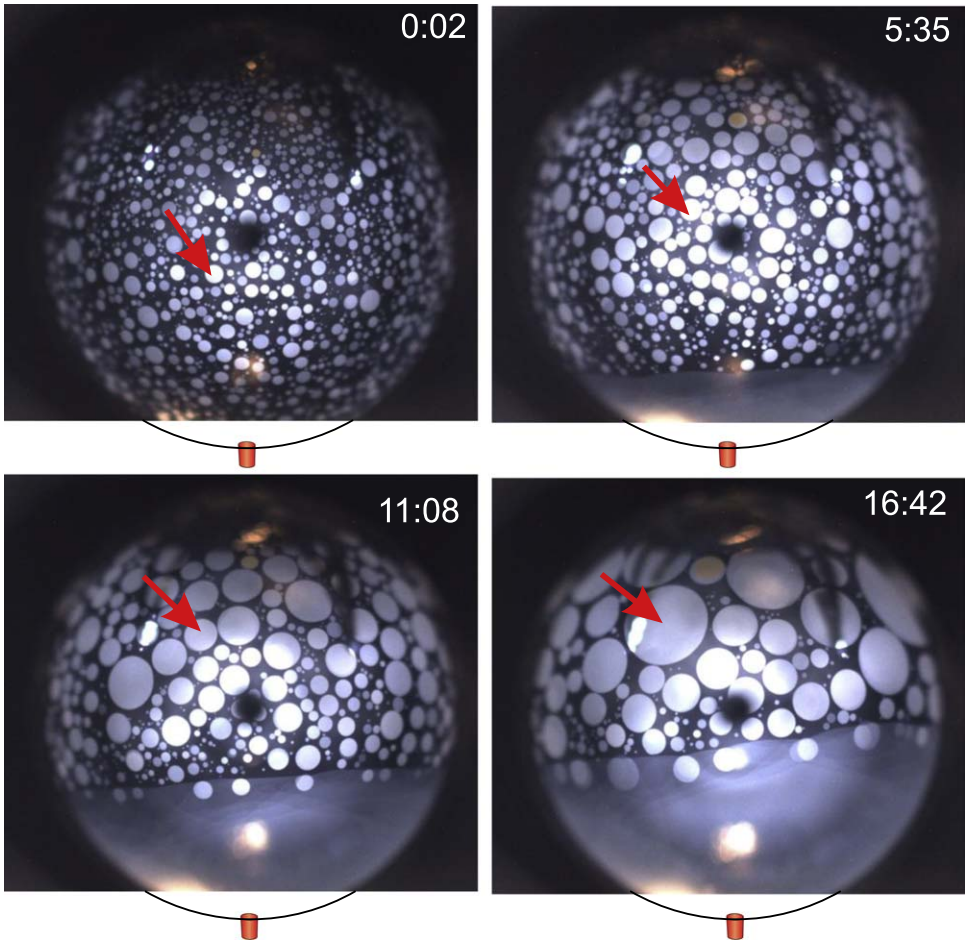

Figure 4. Islands on a smectic bubble migrating under the influence of a thermal gradient (needle at 40 °C, chamber walls at 28 °C). The material is a commercial smectic A mixture (see text). A selected island is marked by arrows to indicate the upward drift. The dark spot facing the observer is a technical artefact. The position of the heated needle tip is sketched below the images. The images were taken from a sequence recorded at a frame rate of 30 fps. Time is shown in the form min:s in each image.

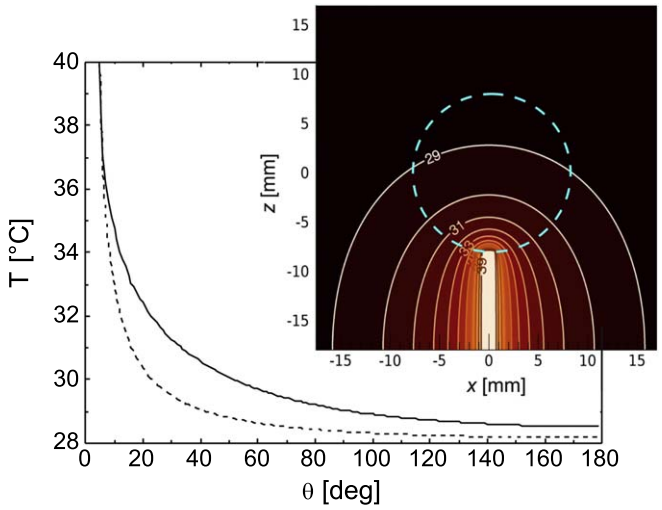

Figure 5. Calculated temperature profile at the smectic bubble surface established by heat conduction of the ambient air, with the supporting needle at 40 °C and the chamber walls at 28 °C. The solid curve represents the numerically computed profile. For comparison, the dashed curve shows the analytical result for a spherical heat source with radius r_c at the needle tip. The inset shows the stationary, axially symmetric solution of the heat diffusion equation, with contour lines in 2 K steps. The bubble is indicated by the dashed circle.

the computed temperature profile of the smectic film, as a function of the polar angle defined in figure 1(c). The dashed curve shows for comparison the analytical solution of the temperature distribution assuming a heated sphere with the diameter of the support capillary, $2r_c$, located at its tip, in the center of a spherical chamber. The average temperature gradient along the bubble surface is of the order of 1 K mm^{-1} but it is very inhomogeneous: in the vicinity of the support needle, the gradient reaches 10 K mm^{-1}. This is comparable to the gradients imposed in the TEXUS experiments (section 2.1). Across the upper hemisphere of the bubble, the temperature difference barely exceeds 1 K. The inset shows the complete temperature profile in the chamber, with isotherms in 2 K steps. The dashed blue circle represents the smectic bubble supported by the needle.

The temperature gradient causes film material to flow from the meniscus around the needle into the bubble. The thin background film is gradually replaced by thicker, hotter film, about 50–80 nm in thickness. This drift raises the temperature of the film, modifying the local temperature distribution. The increased film temperature (a few mK) leads to a reduced surface energy [32]. The temperature coefficient of surface tension of the mesogenic mixture used in the experiment has not been measured, but we assume that it is of the same order of magnitude as a number of other LCs with similar structures [29], $\mathrm{d}\sigma/\mathrm{d}T \approx -5 \times 10^{-5}$ N m^{-1} K^{-1}.

The meniscus represents a huge reservoir, its contents far exceeding the volume required to increase the film thickness by dozens of nanometers. The smectic material delivered by the meniscus around the needle pushes the smectic islands upwards. The 'upward' migration of the islands on the bubble is apparent in figure 4. A thick film region that originates around the needle and advances 'northward', occupying more and more of the lower part of the bubble, is captured in the space-time plot of figure 6(a), where one recognizes that the flow involves the complete bubble surface.

For an interpretation of the observed drift of the islands, one needs to consider the experimental geometry. A divergence-free, axially symmetric flow field originating from the meniscus at the support needle would require a velocity $v(\theta) = v_0/\sin\theta$ (definition of θ see figure 1), with a constant v_0 corresponding to the flow velocity at the equator. On the other hand, the projection of v near the vertical mid-plane of the bubble onto the viewing direction yields $v_{\mathrm{app}} = v\sin\theta$. Thus, a non-divergent flow would be manifest in the images in an overall θ-independent upward motion of islands advected with the background film, with an apparent flow velocity $v_{\mathrm{app}} = v_0$. The observed film velocity is larger near the meniscus and decreases towards the equator. Figure 6 (b) compares the apparent velocities at the edge of the thicker region and near the bubble equator over time. The material leaves the meniscus with a velocity of the order of 130 μm s^{-1} at the beginning of the experiment, with this velocity later dropping to about half of the initial value.

When one considers the propagation of the thick film edge in figure 6, one has to be aware that the pressure inside the film is slightly lower (by a few Pascal) than the air pressure outside. Thus a small force pushes the edge towards the thicker film region. Moreover, the upward motion of the thicker region increases the length of the edge, which has a line tension of the order of 50 pN (the product of step height and surface tension). These forces are of similar magnitude, and they act in the same direction. The former increases with $\sin\theta$ during climbing, the second decreases with $\cos\theta$. Relative to the driving thermocapillary forces, however, they can both be safely neglected.

Thermotropic smectic A and smectic C LCs are essentially incompressible fluids. Nevertheless, the 2D flow field on the surface of a tethered smectic bubble is not neccessarily divergence-free. The flow field is complicated by there being a source of LC material around the needle (the meniscus) but no corresponding drain at the opposite pole of the bubble. Excess material that accumulates on the bubble as a result of thermocapillary flow can be absorbed by growing islands with excess layers (escaping to the third dimension). The island coarsening seen in figure 4 is partly a result of coalescence and Ostwald ripening, processes which occur on bubbles in thermal equilibrium as well. However, in the presence of a temperature gradient we observe an increase in the total area of islands resulting from the net influx of smectic material from the meniscus. The divergence of the flow field is reflected in the difference of apparent velocities measured at the edge of the thick region at the bottom and at the bubble equator (figure 6(b)). Note that this divergence does not vanish with time, even though the two curves approach each other. This occurs simply because the bottom island border climbs up and approaches the equator. Figure 6(b) also shows that the climbing velocity of the thick region decreases approximately linearly in time. Assuming that a stationary temperature distribution is established after the first minute, this observation indicates that the thermally driven transport becomes less efficient. The reason is probably that an even thicker film emerges from the meniscus at later stages.

As in the planar films, the flow is limited by the induced stress at the meniscus and the island borders that have to release or absorb, respectively, the transported film material. The relation between the stress p_m at these borders and the velocity v_{in} of the inflow into an island is, as above, $p_m = v_{\mathrm{in}}/m$, with the dislocation mobility m. A similar stress is produced at the meniscus around the supporting needle (see section 2.1). The efficiency of this mechanism is not influenced by the number and mean size of islands, because the absolute volume of absorbed material per time is independent of these quantities as long as the outflow from the meniscus is constant.

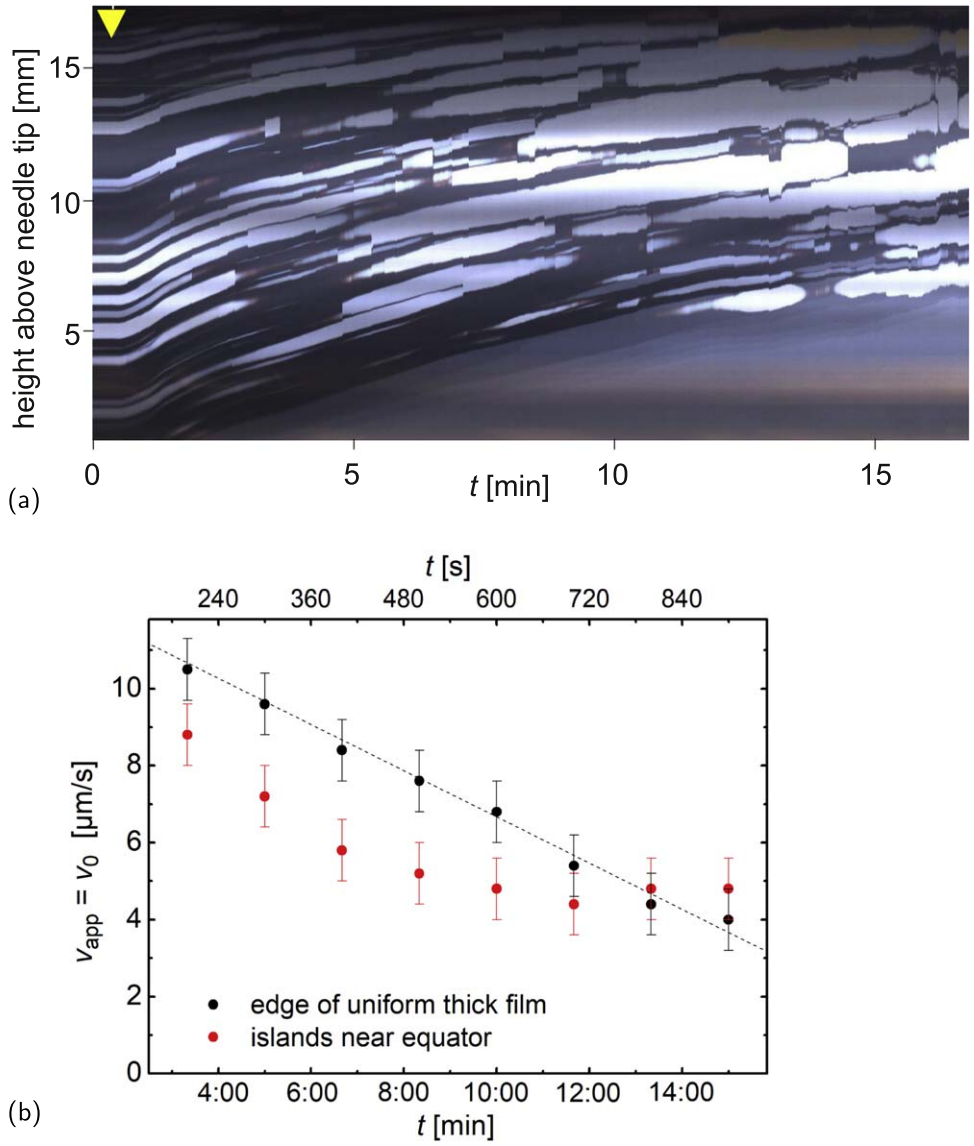

Figure 6. (a) Space-time plot of the vertical profile of the image sequence from figure 4, obtained 2 mm left of the center (immediately left of the black artifact in the images). The time axis runs from 0:00 to 16:47 min, the vertical axis covers 15 mm, where the bottom is 1 mm above the needle tip and the top is the upper end of the bubble. The chamber walls were at 28 °C. The temperature of the needle was changed from 28 °C to 40 °C at time 0:24 min (yellow arrow). (b) Velocities v_{app} of the edge of the thick advancing region at the bottom and island near the equator of the bubble, the dashed line is a linear fit.

A complete, quantitative analysis of the bubble observations is challenging because of the complex geometry of the experiment. However, we note that the measured flow velocity at the capillary, $v_c \approx v_0 r_b / r_c \approx 130$ μm s^{-1}, with a temperature gradient near the needle of $\approx$1 K mm^{-1}, is rather similar to that measured in the TEXUS experiments with flat films with well-defined geometry and gradients [32]. This provides some confidence that flow is caused by the same mechanism, and that the two smectic materials behave qualitatively similarly.

Marangoni flow in the opposite direction, *towards* the supporting needle, was achieved by setting that needle to the chamber temperature and heating the two metal airjet needles at the opposite pole of the smectic bubble [31]. Selected images of this experiment are shown in figure 7. The gradient is imposed by heating a pair of needles (indicated in yellow) above the bubble to 45 °C, with the bubble chamber at 30.5 °C. This case is essentially different from the other experiments described in this paper: The film is heated without direct contact, in an area where no reservoir in the form of a meniscus is available. The film material again flows from the hot polar region toward the cold one, with an initial apparent velocity of about 25 μm s^{-1} estimated from the displacement of dark 'holes' (regions of lower film thickness) that form around the top of the bubble. Since there is no reservoir that can deliver liquid crystalline material, the film compensates for the divergent 2D flow by thinning the upper part of the bubble, leading, eventually, to the growth of a large hole. Only a few smectic layers remain in this region, the hole appearing nearly black in the images (figures 7(a)–(d)). The hole expands during

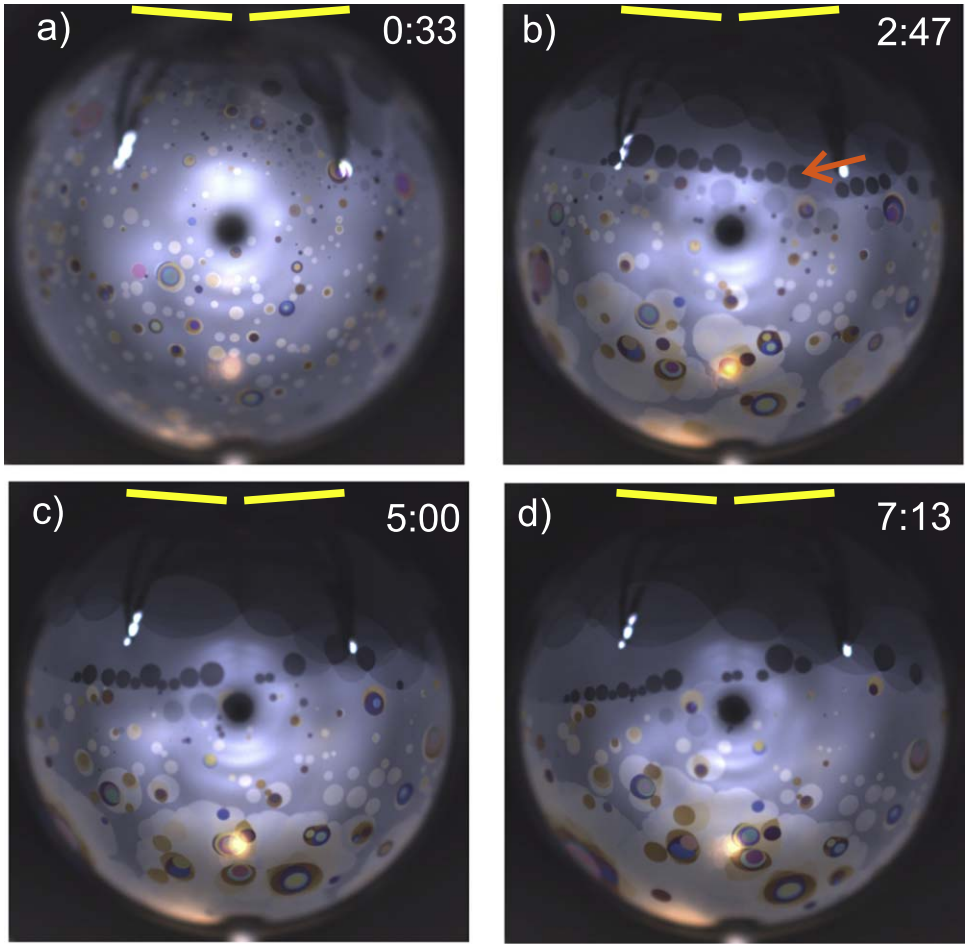

Figure 7. Islands on a smectic bubble migrating under the influence of a thermal gradient (heated needles above the bubble top, indicated schematically by yellow lines, at 45 °C, bubble chamber at 30.5 °C). The dark spot facing the observer is a technical artefact. The images were taken from a 10 min sequence recorded at a frame rate of 30 fps. Time is shown in the form min:s in each image. The red arrow marks a typical 'hole', a region with reduced film thickness.

the first 3 min of the applied temperature gradient but then the expansion stops (figures 7(c), (d)). This can be explained as follows: as long as there is a significant temperature gradient outside the hole, the thin film region can expand and thereby generate flow in the gradient region. Once the hole has expanded to cover the thermally inhomogeneous part of the bubble, there is no further expansion (because a further expansion of the thin region would promote flow only in film areas that are nearly constant in temperature, with no reduction of surface energy). Inside the very thin hole, temperature gradients do not generate flow because this would require further film thinning. The described thermal mechanism does not provide enough energy to nucleate new, thinner holes. One would presumably need to heat the film by another 10 K, close to the nematic phase transition in order to induce layer thinning [35], and to move more material away from the hot pole.

2.3. Climbing of smectic layers in vertical films

The geometry of vertical smectic films under normal gravity, studied by Birnstock [30], adds even more complexity. First, the gravitational forces themselves that act on the film material have to be considered, and second, the films are in general inhomogeneous after preparation, with a vertical thickness gradient. If a thermal gradient is applied between a lower hot frame edge and an upper cold edge, thermally induced flow transports smectic layers upwards against the gravitational drag. A suitable extended model must include not only the additional external forces, but also the dynamics of the film thickness profile, i.e. the motion of dislocations relative to the flowing film material. Within the present paper, we provide only a qualitative discussion of this experiment, without a quantitative analysis which would require the solution of the Navier–Stokes equation in the film with the appropriate boundary conditions.

Figure 8 shows images of a vertical film with a width of 33 mm and a height of 20 mm in the geometry of figure 1(b). In the upper part, where the film is thinnest (≈80 nm), buoyancy-driven thermoconvection of ambient air induces vortex flow in the film by advection. This is seen in the early images of figure 8 where some islands are distorted and carried along with two counter-rotating convection rolls. In this region, the

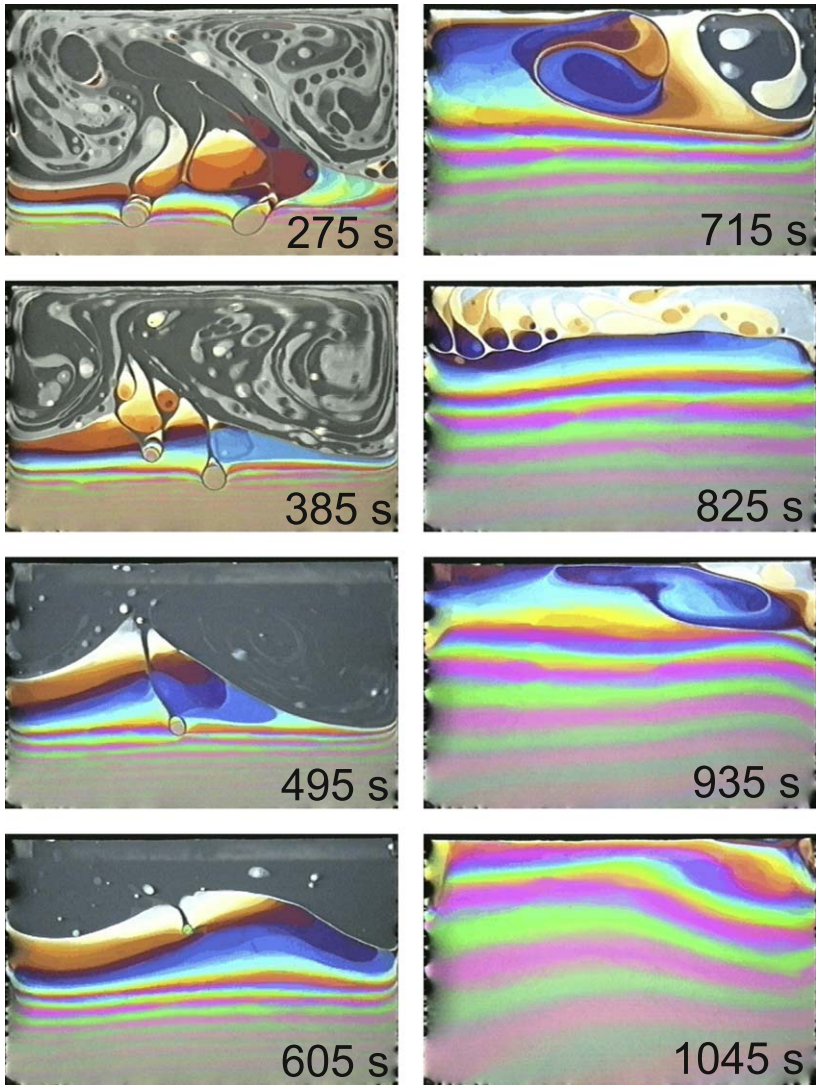

Figure 8. Climbing of smectic layers in a vertically suspended film under the influence of a vertical temperature gradient. A thermostated block at the lower frame edge was set to a temperature of $T_h = 70$ °C. The top of the frame was not heated. It remained approximately at room temperature (25 °C). Images are 33×20 mm^2. The smectic material is the commercial mixture FELIX16-100 (*Hoechst*). During the first 10 min, hot air flowing upwards induces a pair of convection rolls in the upper thin film region (thickness ≈80 nm). The thicker regions that climb up are less sensitive to air flow, thus the convection ceases.

temperature gradient is averaged out to a large extent by the convective flow. However, the differences in surface tension at the top and bottom edges of the frame still act on the film as a whole and move the film material upwards, against the thermal gradient. In figure 9 we have traced the positions of film regions of constant thickness, which are identified by their interference colors. Initially, the overall upward drift is faster than the motion of dislocations relative to the film, and the thicker regions in the lower parts of the film climb upwards. This reverses after some time in the lower parts (thicker film regions). This can be attributed to the competition of two effects: gravitation forces pull the excess layers down, against the thermally induced drift. The thermocapillary forces pull the film material up, towards the colder edge. The thermocapillary effects are more efficient for thinner film regions (see equation (1)). The observed displacement of regions of constant thickness is thus the superposition of two motions, an upward material transport and a downward shift of dislocations relative to the film material. We cannot distinguish these two processes since in unpolarized light, the textures as indicators of material transport are not visible. The actual upward material transport may therefore be substantially larger than the climbing velocities plotted in figure 9.

Qualitatively, the trends of the graphs in figure 9 can be explained as follows: Initially, when the film at the top was very thin, the thermally induced drift was faster than the relative downward motion of dislocations everywhere in the film. Therefore, all graphs in the plot rise. When the thicker film regions reached the top edge, the inflow decelerated with larger film thickness (equation (1)). Additionally, the temperature of the upper frame edge may have increased slightly, reducing the effective temperature gradient. As a consequence, the Marangoni flow slowed down and the downward dislocation motion took over, starting in the thickest film parts.

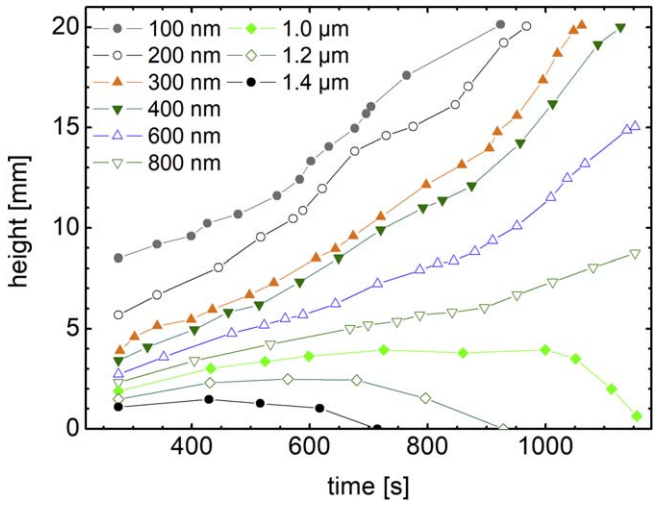

Figure 9. Climbing of smectic layers in the film shown in figure 8. Since the zones of equal thickness are not exactly horizontal but perturbed by convection, the heights represent averages over width of the film.

Additionally, the mutually repulsive interactions of dislocations may play a role in the broadening of the film thickness gradient.

The observations presented in figure 8, obtained in an experiment almost two decades ago, demonstrate that the Marangoni effect is powerful enough to overcome gravitation forces in thin films. However, Birnstock's experiment in 2001 had a different focus, and the setup was not designed for quantitative analysis. Since the upper frame edge was not thermostated, it can only be assumed that it was at a temperature close to, but not exactly equal to, room temperature. For a quantitative investigation of this phenomenon, further experiments under well-controlled thermal conditions are needed.

Irrespective of that, one can estimate the temperature gradients that are needed to lift smectic film material by thermocapillary forces: the difference in gravitational (hydrostatic) pressure between the top and bottom film edges is $\Delta p_{\mathrm{grav}} \leqslant \rho g H$, where ρ is the smectic mass density and H is the vertical film height. The equality sign holds for a uniformly thick film, in films with vertical thickness gradient $\mathrm{d}h/\mathrm{d}z < 0$, the pressure difference is smaller. The pressure generated by capillary forces is $\Delta p_{\mathrm{c}} = 2\Sigma\theta H/h$, with the temperature coefficient of the surface tension, $\Sigma \approx -5 \times 10^{-5}$ N Km^{-1}, for the smectic mixture used [29] and the vertical temperature gradient $\theta = \Delta T/H$. The condition $\Delta p_{\mathrm{c}} > \Delta p_{\mathrm{grav}}$ is fulfilled when

$$\theta > \frac{\rho g h}{2\Sigma}. \tag{2}$$

For a film with thickness $h = 1$ μm, the minimal temperature gradient for upward transport is approximately 0.1 K mm^{-1}. With larger gradients, the smectic film material can be lifted to considerable heights by thermocapillary forces (as long as the temperature remains in the smectic phase range). In the experiment shown in figure 8, the temperature gradient was of the order of 2 K mm^{-1}. The temperature difference would have sufficed to lift film material by about 40 cm, i.e. much more than the actual frame height. The actual value of θ was probably lower in that experiment, because the temperature of the upper frame edge was not measured, and because we have disregarded the temperature drop in the large menisci that are present in this setup. We can nevertheless conclude that for this particular set of parameters, gravitation forces lead only to minor corrections of the Marangoni effect, and the experiment would essentially work quite similarly in a horizontal film. The calculated hydrostatic pressure difference is $\Delta p_{\mathrm{grav}} < 200$ Pa, while Δp_{c} may be of the order of 4 kPa.

In relation to the thermocapillary forces acting on the film, its momentum changes and related kinetic energy changes are negligibly small. For example, the acceleration of a 1 μm thick film in the frame from rest to the maximum velocity observed in the experiment ($\approx$30 μm s^{-1}) within 1 second would require a pressure of less than 1 mPa on one of the frame edges only. The same holds for the acceleration of additional meniscus material entering the film when its thickness increases on the time scale of the experiment. This means that, as in the other experiments described above, the energy gained by capillary forces is dissipated almost completely in the film and the menisci, by the motion of dislocations.

In the study of Birnstock [30], it was further reported that excess smectic material transported in a vertical homogeneously thick film accumulated at the upper, cold edge of the film. In contrast to the films observed in microgravity, the thick bulge at this cold top edge became unstable (Rayleigh–Taylor instability) and droplets trickled back down the film. This process continued as long as the temperature gradient was maintained.

3. Summary and conclusions

The principal mechanism that is responsible for flow in freely suspended smectic films with in-plane temperature gradients has been discussed in a previous publication [32]. Here, we reviewed several experiments where thermocapillary flow in free-standing smectic films transports material and inclusions, in different geometries, with and without gravitation.

The evaluation of video data of the TEXUS 52 suborbital rocket experiments in microgravity, presented in section 2.1, has not only demonstrated that mesogenic material accumulates in large quantities at the colder edge of the film, it has also shown that the flow can produce stress that affects the compression or relaxation of film regions containing dislocation arrays (wedge-shaped regions). The rate of this process is determined by the balance of thermocapillary forces at the thermocontacts in the film and hydrodynamic dissipative forces related to the dislocations that are formed and transported when the film material enters or leaves the menisci.

Spherical smectic films decorated with 2D emulsions of islands were investigated in temperature gradients during the OASIS mission on the International Space Station, with results presented in section 2.2. Local heating of the smectic bubbles in microgravity generates thermocapillary forces that drive flow in the film. The directed motion of smectic islands under thermal gradients that is found in these experiments (figure 4) is at first glance reminiscent of thermomigration or thermophoresis observed in suspensions, emulsions or mixtures of fluids. In fact, however, the islands simply move with the background film, and their motion is not the consequence of direct interactions with the thermal gradient. Holes in the flowing film move in the same direction as islands (figure 7), also being carried away from the high temperature region, with the background film. The islands or holes can thus serve as tracers that indicate the local film drift.

Direct interactions of islands or holes with thermal gradients in the film plane may exist as well, but these are much weaker: one could imagine, for example, forces that drive dislocations that surround islands or holes towards hotter film regions where the liquid-crystalline order parameters are lower. Such forces would act opposite to the observed direction of motion. We expect them to be negligibly small compared to the thermocapillary drift forces.

The OASIS experiments demonstrated that Marangoni flow of the film can transport inclusions, which could be exploited in practical applications. For example, such inclusions could be droplets of reactants for chemical reactions or microprobes in chemical sensors. The experiments also demonstrate that direct contact between the smectic film and the heat source is not needed. When the film is heated in a region far from a reservoir (meniscus), such as in bubbles heated at the end furthest from the support needle (figure 7), material is transported against the temperature gradient as long as the film is inhomogeneously thick there. Then, the hot region can grow by an expansion of existing holes or by the shrinkage of islands. Further growth of a homogeneous film region would require the creation of new holes by thermocapillary forces.

Finally, we have shown that even moderate temperature gradients can be sufficient to lift smectic material in a vertical film against normal gravity. Since the relative strengths of capillary and gravitational forces depend on the film thickness (equation (2)), films a few nm in thickness will be particularly susceptible to even very small temperature gradients of the order of 1 mK mm^{-1}. This has to be taken into account in all situations where local heat sources affect smectic films, for example when absorption processes of films doped with dyes play a role or when chemical reactions take place. The calculation of the dynamics of inhomogeneous vertical films is a challenging future task, and its experimental investigation requires an improved setup with well-defined boundary conditions. Tracking the motion of small, neutrally-buoyant objects in the film may help to distinguish the motion of dislocations from transport of film material.

Marangoni flow should be taken into account in all situations where smectic films are not held under isothermal conditions. It may also be exploited in microfluidic applications.

Acknowledgments

The Magdeburg group was supported by the German Aerospace Center (DLR) within projects 50WM1430 and 50WM1744 (OASIS-Co) and by the Deutsche Forschungsgemeinschaft (DFG) within project STA 425/40-1. The authors are particularly indebted to the DLR for making the TEXUS experiments possible, and to Airbus DS for the construction and testing of the equipment as well as for their technical support during the TEXUS-52 and TEXUS-55 campaigns at Esrange. The Colorado group was supported by NASA Grant NNX-13AQ81G and by the Soft Materials Research Center under NSF MRSEC Grant DMR-1420736. CK acknowledges support from a Landesstipendium Sachsen-Anhalt.

References

[1] Young C Y, Pindak R, Clark N A and Meyer R B 1978 Light-scattering study of two-dimensional molecular-orientation fluctuations in a freely suspended ferroelectric liquid-crystal Film *Phys. Rev. Lett.* **40** 773
[2] Rosenblatt C, Pindak R, Clark N A and Meyer R B 1979 Freely suspended ferroelectric liquid-crystal films: absolute measurements of polarization, elastic constants, and viscosities *Phys. Rev. Lett.* **42** 1220
[3] Stoebe T and Huang C C 1995 Physical properties of thin substrate-free liquid-crystal films *Int. J. Mod. Phys.* **9** 1185
[4] Fera A *et al* 2000 Complex dynamic behavior of fluctuating smectic-A films as studied by scattering with coherent x-rays *Phys. Rev. Lett.* **85** 2316
[5] de Jeu W H, Ostrovskii B I and Shalaginov A N 2003 Structure and fluctuations of smectic membranes *Rev. Mod. Phys.* **75** 181
[6] Dolganov P V, Zhilin V M, Dolganov V K and Kats E I 2003 Structures and phase transitions in polar smectic liquid crystals *Phys. Rev.* E **67** 041716
[7] Oswald P and Pieranski P 2005 *Smectic and Columnar Liquid Crystals: Concepts and Physical Properties Illustrated by Experiments* (Milton Park: Taylor and Francis)
[8] Cladis P E, Couder Y and Brand H R 1985 *Phys. Rev. Lett.* **55** 2945
[9] Link D R *et al* 2000 Ring-pattern dynamics in smectic- C^* and Smectic- C^*_A freely suspended liquid crystal films *Phys. Rev. Lett.* **84** 5772
[10] Stannarius R, Bohley C and Eremin A 2006 Vortex flow in free standing smectic films driven by elastic relaxation of the c-director *Phys. Rev. Lett.* **97** 97802
[11] Nguyen Z H, Atkinson M, Park C S, Maclennan J, Glaser M and Clark N 2010 Crossover between 2D and 3D fluid dynamics in the diffusion of islands in ultrathin freely suspended smectic films *Phys. Rev. Lett.* **105** 268304
[12] Eremin A, Baumgarten S, Harth K, Stannarius R, Nguyen Z H, Goldfain A, Park C S, Maclennan J E, Glaser M A and Clark N A 2011 Two-dimensional microrheology of freely suspended liquid crystal films *Phys. Rev. Lett.* **107** 268301
[13] Maclennan J E 1990 Spontaneous director rotation in freely suspended ferroelectric liquid-crystal films *Europhys. Lett.* **13** 435
[14] Morris S W, de Bruyn J R and May A D 1990 Electroconvection and pattern formation in a suspended smectic film *Phys. Rev. Lett.* **65** 2378
[15] Langer C and Stannarius R 1998 Electroconvection in freely suspended smectic-C and smectic-C^* films *Phys. Rev.* E **58** 650
[16] Qi Z Y *et al* 2014 Mutual diffusion of inclusions in freely suspended smectic liquid crystal films *Phys. Rev. Lett.* **113** 128304
[17] Bohley C and Stannarius R 2008 Inclusions in free standing smectic liquid crystal films *Soft Matter* **4** 683 and references therein
[18] Cluzeau P, Poulin P, Joly G and Nguyen H T 2001 *Phys. Rev.* E **63** 031702
[19] Cluzeau P, Joly G, Nguyen H T and Dolganov V K 2002 *J. Exp. Theor. Phys.* **75** 482
Cluzeau P, Joly G, Nguyen H T and Dolganov V K 2002 *J. Exp.Theor. Phys.* **76** 351
[20] Dolganov P V, Shuravin N S, Dolganov V K and Kats E I 2016 Chain structures and clusters of particles with the mixed dipole-quadrupole interaction in smectic freely suspended nanofilms *JETP Lett.* **104** 263
[21] Ben Amar M, da Silva P P, Brazovskaia M, Even C and Pieranski P 1998 Vibrations of smectic films *Phil. Mag.* B **78** 115
[22] Müller F and Stannarius R 2006 Collapse of catenoid-shaped smectic films *Europhys. Lett.* **76** 1102
[23] May K, Harth K, Trittel T and Stannarius R 2012 Dynamics of freely floating smectic bubbles *Europhys. Lett.* **100** 16003
[24] May K, Harth K, Trittel T and Stannarius R 2014 Freely floating smectic films *Chem. Phys. Chem.* **15** 1508
[25] Müller F, Kornek U and Stannarius R 2007 Experimental study of the bursting of inviscid bubbles *Phys. Rev.* E **75** 065302(R)
[26] Trittel T, John Th, Tsuji K and Stannarius R 2013 Rim instability of bursting thin smectic films *Phys. Fluids* **25** 052106
[27] Trittel T, Harth K and Stannarius R 2017 Smectic C to smectic A transition induced mechanically by the rupture of freely suspended liquid crystal films *Soft Matter* **13** 3199
[28] Godfrey M I and van Winkle D H 1996 Surface-tension-gradient-induced flow in freely suspended liquid crystalline films *Phys. Rev.* E **54** 3752
[29] Schüring H, Thieme C and Stannarius R 2001 Surface tensions of smectic liquid crystals *Liq. Cryst.* **28** 241
[30] Birnstock J and Stannarius R 2001 Vertically suspended smectic films with in-plane temperature gradients *Mol. Cryst. Liq. Cryst.* **366** 815
[31] Clark N A *et al* 2017 Realization of hydrodynamic experiments on quasi-2D liquid crystal films in microgravity *Adv. Space Res.* **60** 737
[32] Trittel T, Harth K, Klopp C and Stannarius R 2019 Marangoni flow in freely suspended liquid films *Phys. Rev. Lett.* **122** 234501
[33] Picano F, Holyst R and Oswald P 2000 Coupling between meniscus and smectic-A films: circular and catenoid profiles, induced stress, and dislocation dynamics *Phys. Rev.* E **62** 3747
[34] Cross M C and Hohenberg P C 1993 Pattern formation outside of equilibrium *Rev. Mod. Phys.* **65** 851
[35] Stoebe T, Mach P and Huang C C 1994 Unusual layer-thinning transition observed near the Smectic-A-Isotropic transition in free-standing liquid-crystal films *Phys. Rev. Lett.* **73** 1384